Hindawi Publishing Corporation
Journal of Sensors
Volume 2016, Article ID 6291216, 10 pages
http://dx.doi.org/10.1155/2016/6291216

Research Article

Collision Sensing Using Force/Torque Sensor

Yu-Quan Leng,[1,2] Zheng-Cang Chen,[1,2] Xu He,[1] Yang Zhang,[1] and Wei Zhang[1]

[1]*Department of Space Automation Technologies & Systems, State Key Laboratory of Robotics, Shenyang Institute of Automation, Shenyang 110016, China*
[2]*University of Chinese Academy of Science, Beijing, China*

Correspondence should be addressed to Yu-Quan Leng; lengyuquan@sia.cn

Received 15 June 2015; Accepted 27 August 2015

Academic Editor: Dong-ning Wang

Collision sensing including collision position, collision direction, and force size could make robots smoothly interact with environment, so that the robots can strongly adapt to the outside world. Skin sensor imitates principles of human skin using special material and physical structure to obtain collision information, but this method has some disadvantages, such as complex design, low sampling rate, and poor generality. In this paper, a new method using force/torque sensor to calculate collision position, collision direction, and force size is proposed. Detailed algorithm is elaborated based on physical principle and unified modeling method for basic geometric surface. Gravity compensation and dynamic compensation are also introduced for working manipulators/robots in gravity and dynamic environment. In addition, considering algorithm solvability and uniqueness, four constraints are proposed, which are force constraint, geometric constraint, normal vector constraint, and current mutation constraint. In order to solve conflict solution of algorithm in redundant constraints, compatibility solution analysis is proposed. Finally, a simulation experiment shows that the proposed method can achieve collision information efficiently and accurately.

1. Introduction

In recent years, more and more sensors are installed on robots to realize sensing and interacting with environment. These sensors help robots achieve a large amount of information about the environment, which contributes robots to make correct decision and planning. For example, vision sensor assists robots in obtaining appearance information of environment, which is used to realize target tracking and object capture, and so forth.

Collision sensing is also an important environment sensing method, through which robots sense collision point and collision direction to avoid collision again, and makes compliment control come true [1, 2]. In the environment containing human and robots, collision sensing is extremely significant to avoid serious collision. In addition, in [3], collision sensing is also used for compliance assembly. Since that collision sensing has so many applications, realization of whole robotic body sensing is gradually carried out [4, 5].

Skin force sensor like human skin system, which is pasted on the whole surface of robots, could sense force action point, force direction and size [2, 5]. In the research filed, MIT has developed a special compound material called QTC (Quantum Tunneling Composite), which is pressed by metal and nonmetal [2, 6]. This sensor measures force information by resistance change when it is pressed. Similar researches also include organic thin film composed of pentacene molecular (U-Tokyo, Japan) and E-skin (Philips Company), and so forth [1]. The skin force sensor looks like an ideal solution for robot force sensing, but there are many disadvantages that make it hard to be used in real world, such as being easy to damage during collision, expensive price, complex design and high environment requirements, low sampling rate, and poor generality [4, 7]. Moreover, sensitivity of skin sensor system could not achieve information of collision direction and could be influenced by many factors, such as temperature and humidity [1].

Skin force sensor is the direct method to measure force information; on the other way, it also could be checked out through indirect techniques [8, 9]. In [10] Mason and Salisbury have proposed the theory of calculating force information using force/torque sensor and in [11] Bicchi et al. have developed experiments to verify it. Zhou and Han use the theory to realize skin force sense on the one

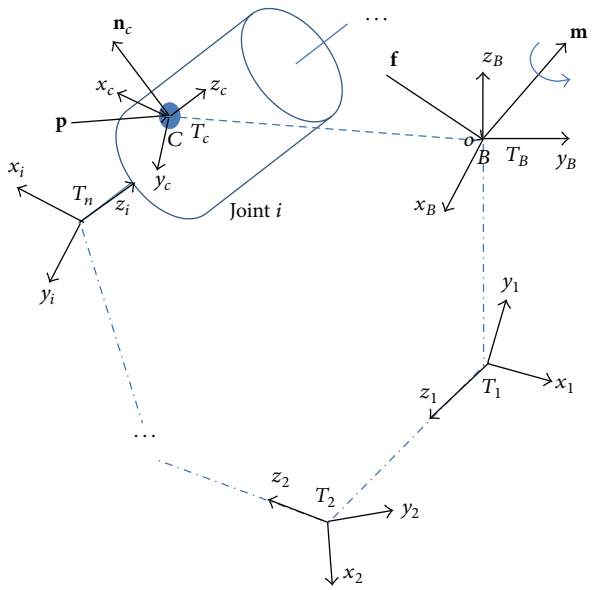

FIGURE 1: Collision analysis.

freedom finger [12–14]. In this paper, theories of manipulator with multiple degrees of freedom are applied and method of compatibility solution analysis to solve contradiction of solutions is proposed.

The rest of this paper is organized as follows. Section 2 describes detection principle, when point collision happens, unified equation for collision sensing considering gravity and manipulator dynamics, and unified modeling method for basic geometric surface. In the gravity environment, force analysis is proposed in Section 3. In Section 4, force analysis is shown when manipulator is in a working condition. Solvability analysis is provided in Section 5, which includes force constraint, geometric constraint, normal vector constraint, current mutation constraint, and compatibility solution analysis. In Section 6, the simulation experiment and results are shown to prove effectiveness of the algorithm. Finally, the concluding remarks follow in Section 7.

2. Detection Principle

In this section, physical principle about point collision on manipulator is introduced. On the one hand, the whole process of force effect needs meets force analysis principle, and on the other hand, the result of calculation should suit physical laws, such as point c which is on the manipulator surface and the angle of force direction and normal vector is less than $\pi/2$.

2.1. Force Analysis. Assume that no gravity and manipulator are static; force analysis is shown in Figure 1. In order to apperceive whole system, force/torque sensor is assembled on the base and close to the first joint. The force/torque sensor could measure force in three directions and torque rotated of three coordinate axes.

In Figure 1, point C means collision point, which is assumed on ith joint. The center of force/torque sensor is expressed as B, which is set as origin of B coordinate system. Every joint of manipulator is built coordinate system as T_i according to DH parameter method. T_i represents coordinate system of ith joint, and $\mathbf{p}$, $\mathbf{f}$, and $\boldsymbol{\tau}$, respectively, mean collision force, measured force, and measured torque. $\mathbf{n}_c$ represents normal vector of point c. T_c could be achieved by translating coordinate system T_i and no rotation. Then coordinate of point C in T_B is obtained by coordinate transformation, as shown in the following:

$$ {}^{c}_{B}\mathbf{T} = {}^{1}_{B}\mathbf{T}\,{}^{2}_{1}\mathbf{T}\cdots{}^{i}_{i-1}\mathbf{T}\,{}^{c}_{i}\mathbf{T}, \tag{1} $$

where

$$ {}^{i-1}_{i}\mathbf{T} = \begin{bmatrix} c\theta_i & -s\theta_i c\alpha_i & s\theta_i s\alpha_i & a_i c\theta_i \\ s\theta_i & c\theta_i c\alpha_i & -c\theta_i s\alpha_i & a_i s\theta_i \\ 0 & s\alpha_i & c\alpha_i & d_i \\ 0 & 0 & 0 & 1 \end{bmatrix}, $$
$$ {}^{c}_{i}\mathbf{T} = \begin{bmatrix} 1 & 0 & 0 & x_{ic} \\ 0 & 1 & 0 & y_{ic} \\ 0 & 0 & 1 & z_{ic} \\ 0 & 0 & 0 & 1 \end{bmatrix}. \tag{2} $$

When collision occurs, the outside force is $\mathbf{p} = (f_{cx}, f_{cy}, f_{cz})^T$, and data of force/torque sensor are $\mathbf{f} = (f_x, f_y, f_z)^T$ and $\boldsymbol{\tau} = (\tau_x, \tau_y, \tau_z)^T$. According to force analysis, data of outside force in T_B should be equal to measured data in ideal condition, as shown in the following:

$$ \begin{aligned} \mathbf{f} &= \mathbf{f}_{cB}, \\ \boldsymbol{\tau} &= \boldsymbol{\tau}_{cB}, \end{aligned} \tag{3} $$

where

$$ \mathbf{f}_{cB} = \left(f_{cBx}, f_{cBy}, f_{cBz}\right)^T = \left(T\left(\overline{\mathbf{p}}^T\,{}^{c}_{B}\mathbf{T}\right)_{3,1}\right)^T, \tag{4} $$

$$ \boldsymbol{\tau}_{cB} = \left(\tau_{cBx}, \tau_{cBy}, \tau_{cBz}\right)^T = \mathbf{c}_B \times \mathbf{p} = \left(T\left(\overline{\mathbf{c}}_i\,{}^{c}_{B}\mathbf{T}\right)_{3,1}\right) \times \mathbf{p}. \tag{5} $$

In (4),

$$ \overline{\mathbf{p}} = \left(f_{cx}, f_{cy}, f_{cz}, 1\right)^T \tag{6} $$

and $T(\cdot)_{3,1}$ means extraction of elements of the first three rows and the first column.

In (5),

$$ \overline{\mathbf{c}}_i = \left(x_{ci}, y_{ci}, z_{ci}, 1\right)^T. \tag{7} $$

Considering factor of gravity and manipulator dynamics in real world, general equation could be shown as follows:

$$ \begin{aligned} \mathbf{f} &= \mathbf{f}_{cB} + \mathbf{f}_{GB} + \mathbf{f}_{dB} \\ \boldsymbol{\tau} &= \boldsymbol{\tau}_{cB} + \boldsymbol{\tau}_{GB} + \boldsymbol{\tau}_{dB}. \end{aligned} \tag{8} $$

In (8), $\mathbf{f}_{cB}$ and $\boldsymbol{\tau}_{cB}$, respectively, express force and torque caused by collision mapping in basic coordinate system B;

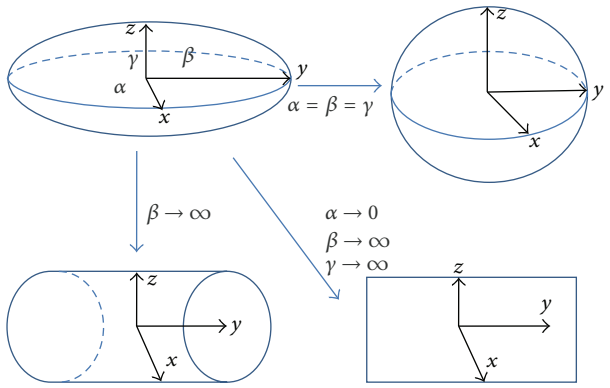

FIGURE 2: Unified modeling method for basic geometric surface.

$\mathbf{f}_{GB}$ and $\boldsymbol{\tau}_{GB}$, respectively, mean force and torque caused by gravity mapping in basic coordinate system B, which will be analyzed in Section 3; $\mathbf{f}_{dB}$ and $\boldsymbol{\tau}_{dB}$, respectively, express force and torque caused by manipulator dynamics mapping in basic coordinate system B, which will be shown in Section 4.

In (8), $\mathbf{f}_{GB}$, $\boldsymbol{\tau}_{GB}$, $\mathbf{f}_{dB}$, and $\boldsymbol{\tau}_{dB}$ could be calculated based on states of manipulator and joint physical properties, such as joint angle, joint velocity, joint acceleration, and joint quality. Collision information is just contented in $\mathbf{f}_{cB}$ and $\boldsymbol{\tau}_{cB}$, that is, the parameters of f_{cx}, f_{cy}, f_{cz}, x_{ci}, y_{ci}, and z_{ci}.

2.2. Physical Constraint. Normal geometrical surface contains ellipsoid, sphere, cylindrical surface, and plane. They are able to construct all simple surfaces including outline of manipulators. Mathematical description mode of all manipulator surface is achieved through coordinate transformation. From the role of geometrical change, the core of four types of surface is ellipsoid, which is able to change to other three types by changing parameters, as shown in Figure 2.

Assume three axis lengths of ellipsoid are 2α, 2β, and 2γ, setting center as origin of coordinate system. When $\alpha = \beta = \gamma$, sphere will be formed; when $\gamma \to +\infty$, cylindrical surface is achieved; and when $\alpha \to +\infty$, $\beta \to 0$, and $\gamma \to \infty$, plane surface is displayed. In summary, it just needs to build ellipsoid mode to describe all surface, as shown in the following:

$$S(\mathbf{c}) = \mathbf{c}^T \mathbf{A}^T \mathbf{A}\mathbf{c} = 1, \tag{9}$$

where

$$\mathbf{A} = \begin{bmatrix} \frac{1}{\alpha} & 0 & 0 \\ 0 & \frac{1}{\beta} & 0 \\ 0 & 0 & \frac{1}{\gamma} \end{bmatrix}. \tag{10}$$

Normal vector of point C is set as $\mathbf{n}_c$ and could be calculated with equation as follows:

$$\mathbf{n}_c = \frac{\nabla S(\mathbf{c})}{\|\nabla S(\mathbf{c})\|} = \frac{2\mathbf{A}^2\mathbf{c}}{\|2\mathbf{A}^2\mathbf{c}\|} = \frac{\mathbf{A}^2\mathbf{c}}{\|\mathbf{A}^2\mathbf{c}\|}, \tag{11}$$

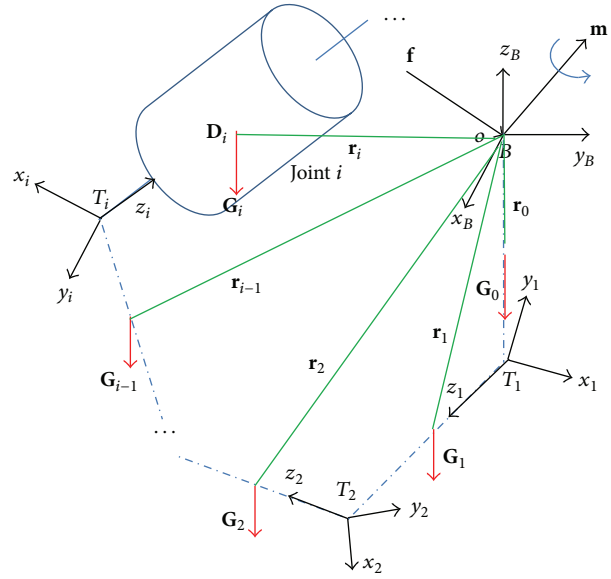

FIGURE 3: Gravity analysis.

where $\mathbf{c} = (x, y, z)$ means coordinate values and ∇ represents gradient.

3. Gravity Compensation

In the above section, gravity element is sampled as $\mathbf{f}_{GB}$ and $\boldsymbol{\tau}_{GB}$. In this section, gravity influence on sensor will be analyzed, which relates to joint length, joint angle gravity center of joint, and quality. All joints cause force and torque on sensor, so each of them needs to be calculated. Force analysis is shown in Figure 3 in gravity.

In Figure 3, $\mathbf{D}_i = (x_{di}, y_{di}, z_{di})^T$ is gravity center position in T_i coordinate; then $\mathbf{r}_i$ means coordinate of gravity center of ith joint and is expressed as

$$\mathbf{r}_i = \left(T\left({}^i_B\mathbf{T}\overline{\mathbf{D}}_i\right)_{3,1}\right)^T, \tag{12}$$

where

$$\overline{\mathbf{D}}_i = (x_{di}, y_{di}, z_{di}, 1)^T. \tag{13}$$

Assuming variety of sensors is $\mathbf{f}_{GB} \in R^3$, $\boldsymbol{\tau}_{GB} \in R^3$, then (14) and (15) are achieved:

$$\mathbf{f}_{GB} = \mathbf{G}_0 + \mathbf{G}_1 + \mathbf{G}_2 + \cdots + \mathbf{G}_i + \cdots + \mathbf{G}_n = \sum_{i=0}^{n} \mathbf{G}_i, \tag{14}$$

$$\begin{aligned} \boldsymbol{\tau}_{GB} &= \mathbf{r}_0 \times \mathbf{G}_0 + \mathbf{r}_1 \times \mathbf{G}_1 + \cdots + \mathbf{r}_i \times \mathbf{G}_i + \cdots + \mathbf{r}_n \\ &\quad \times \mathbf{G}_n = \widehat{\mathbf{G}}_0\mathbf{r}_0 + \widehat{\mathbf{G}}_1\mathbf{r}_1 + \cdots + \widehat{\mathbf{G}}_i\mathbf{r}_i + \cdots + \widehat{\mathbf{G}}_n\mathbf{r}_n \\ &= \sum_{i=0}^{n} \widehat{\mathbf{G}}_i\mathbf{r}_i. \end{aligned} \tag{15}$$

In (14), $\mathbf{G}_i = (0, 0, G_i)^T$ $(i \le n)$ and n is the total number of joints.

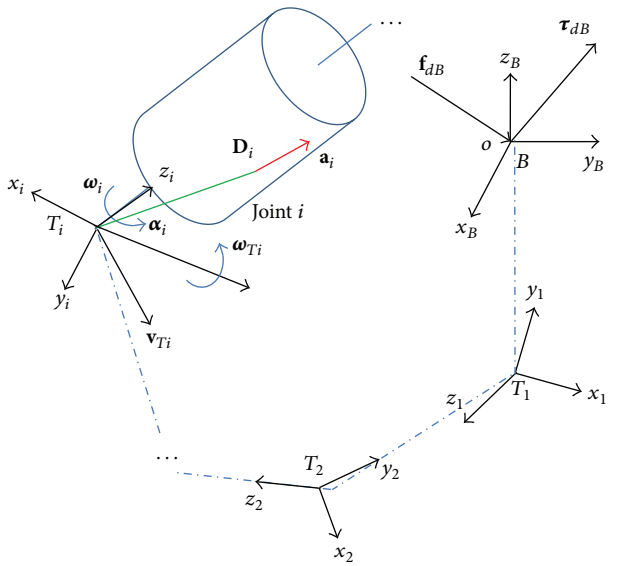

Figure 4: Dynamic force analysis.

In (15), in order to easily calculate with matrix, vector $\mathbf{G}_i$ is transformed into matrix $\widehat{\mathbf{G}}_i$:

$$\widehat{\mathbf{G}}_i = \begin{bmatrix} 0 & 0 & -G_i \\ 0 & 0 & 0 \\ G_i & 0 & 0 \end{bmatrix}, \quad (i \le n). \tag{16}$$

4. Dynamic Compensation

In Section 3, manipulator dynamic is sampled as $\mathbf{f}_{dB}$ and $\boldsymbol{\tau}_{dB}$. In this section, dynamic factor is analyzed. When manipulator works, it also causes reaction force to sensor, so calculation is also needed. Dynamic force is very complex, which relates to joint length, joint angle, joint angular velocity, joint angular acceleration, and so on. In Figure 4, dynamic force is analyzed.

In Figure 4, assume $\boldsymbol{\alpha}_i$ is joint angular acceleration and $\mathbf{D}_i = (x_{di}, y_{di}, z_{di})^T$ is gravity center position in T_i coordinate. Then, acceleration of gravity center is expressed as

$$\mathbf{a}_i = \boldsymbol{\alpha}_i \times \mathbf{D}_i. \tag{17}$$

In T_i coordinate, in order to keep moving as in Figure 4, the force and torque are calculated as shown in the following:

$$\begin{aligned} \mathbf{f}_{di} &= m_i \mathbf{a}_i = m_i \mathbf{a}_i \times \mathbf{D}_i = m_i \widehat{\mathbf{a}}_i \mathbf{D}_i, \\ \boldsymbol{\tau}_{\alpha di} &= \mathbf{I}_i \boldsymbol{\alpha}_i. \end{aligned} \tag{18}$$

In (18), m_i and $\mathbf{I}_i$, respectively, express quality and inertia of ith joint, and

$$\widehat{\mathbf{a}}_i = \begin{bmatrix} 0 & -a_{iz} & a_{iy} \\ a_{iz} & 0 & -a_{ix} \\ -a_{iy} & a_{ix} & 0 \end{bmatrix}. \tag{19}$$

Due to the fact that T_i is a motional coordinate, Coriolis force emerges in the whole system, which is expressed as

$$\mathbf{f}_{kdi} = 2m_i \mathbf{v}_{Ti} \times \boldsymbol{\omega}_{Ti}. \tag{20}$$

In (20), $\boldsymbol{\omega}_{Ti}$ and $\mathbf{v}_{Ti}$, respectively, mean velocity vector and angular velocity vector of T_i coordinate relative to basic coordinate.

Based on the principle of equivalence, the above forces and torque of i joint are transfered to B, which could be expressed as

$$\begin{aligned} \mathbf{f}_{fBdi} &= \left(T\left(\mathbf{f}_{di}^T \, {}_B^D\mathbf{T}\right)_{3,1}\right)^T, \\ \mathbf{f}_{kBdi} &= \left(T\left(\mathbf{f}_{kdi}^T \, {}_B^i\mathbf{T}\right)_{3,1}\right)^T, \\ \boldsymbol{\tau}_{fBdi} &= \mathbf{f}_{fBdi} \times \mathbf{D}_{Bi} = \widehat{\mathbf{f}}_{fBdi}\left(T\left({}_B^i\mathbf{T}\overline{\mathbf{D}}_i\right)_{3,1}\right)^T, \\ \boldsymbol{\tau}_{kBdi} &= \mathbf{f}_{kBdi} \times \mathbf{T}_i = \widehat{\mathbf{f}}_{kBdi}\left(T\left({}_B^i\mathbf{T}\right)_{3,1}\right)^T, \\ \boldsymbol{\tau}_{\alpha Bdi} &= \boldsymbol{\tau}_{\alpha di}. \end{aligned} \tag{21}$$

In the above equation, $\mathbf{f}_{fBdi}$ and $\mathbf{f}_{kBdi}$, respectively, mean acceleration force and Coriolis force in the basic coordinate; $\boldsymbol{\tau}_{fBdi}$ and $\boldsymbol{\tau}_{kBdi}$ express torque of force transformation; torque could transfer with no other changes, so $\boldsymbol{\tau}_{\alpha Bdi} = \boldsymbol{\tau}_{\alpha di}$.

Manipulator contains many joints, so all effect of force of joints on the basic coordinate is shown as

$$\begin{aligned} \mathbf{f}_{dB} &= \sum_{i=1}^{n} \mathbf{f}_{Bdi} = \sum_{i=1}^{n} \left(\mathbf{f}_{fBdi} + \mathbf{f}_{kBdi}\right), \\ \boldsymbol{\tau}_{dB} &= \sum_{i=1}^{n} \boldsymbol{\tau}_{Bdi} = \sum_{i=1}^{n} \left(\boldsymbol{\tau}_{fBdi} + \boldsymbol{\tau}_{kBdi} + \boldsymbol{\tau}_{\alpha Bdi}\right). \end{aligned} \tag{22}$$

5. Solvability Analysis

At present, problem will be analyzed under the following limits in this subsection:

(a) Material of manipulator is rigid, which means no deformation produce.

(b) Collision is caused by manipulator and point of object.

(c) All sensor is ideal.

(d) Gravity is ignored in this subsection, because it has to be calculated in Section 5.3.

(e) Manipulator dynamic is discussed in Section 5.4, so assume manipulator is static and motion of outside object causes collision.

In order to ensure solvability and uniqueness, four constraints are provided and compatibility principle is proposed.

5.1. Force Constraint. From Section 2, combine (8) and (9); seven equations are achieved with six variables. Moreover, $\mathbf{f}_{GB}$, $\boldsymbol{\tau}_{GB}$, $\mathbf{f}_{dB}$, and $\boldsymbol{\tau}_{dB}$ are zero under the above assumption.

In order to easily calculate with matrix, vector $\mathbf{p}$ is transformed into matrix $\widehat{\mathbf{p}}$:

$$\widehat{\mathbf{p}} = \begin{bmatrix} 0 & -f_{cz} & f_{cy} \\ f_{cz} & 0 & -f_{cx} \\ -f_{cy} & f_{cx} & 0 \end{bmatrix}. \tag{23}$$

Then, part of (8) could be changed to

$$\boldsymbol{\tau}_{cB} = \widehat{\mathbf{p}} \left(T \left(\bar{\mathbf{c}}_i \, {}^{c}_{B}\mathbf{T} \right)_{3,1} \right). \tag{24}$$

Combining (1), (8), and (24), the following equation is achieved:

$$\begin{bmatrix} \mathbf{f} \\ \boldsymbol{\tau} \end{bmatrix} = \mathbf{M} \begin{bmatrix} \left(T \left(\bar{\mathbf{p}}^{T} \, {}^{c}_{B}\mathbf{T} \right)_{3,1} \right)^{T} \\ \left(T \left(\bar{\mathbf{c}}_i \, {}^{c}_{B}\mathbf{T} \right)_{3,1} \right) \end{bmatrix}, \tag{25}$$

where

$$\mathbf{M} = \begin{bmatrix} 1 & 0 & 0 & 0 & 0 & 0 \\ 0 & 1 & 0 & 0 & 0 & 0 \\ 0 & 0 & 1 & 0 & 0 & 0 \\ 0 & 0 & 0 & 0 & -f_{cz} & f_{cy} \\ 0 & 0 & 0 & f_{cz} & 0 & -f_{cx} \\ 0 & 0 & 0 & -f_{cy} & f_{cx} & 0 \end{bmatrix}. \tag{26}$$

$\mathbf{M}$ is relation matrix and it is singular matrix in ideal condition, that is, rank($\mathbf{M}$) = 5. A series of solutions about (24) are obtained. There are many states that make rank($\mathbf{M}$) = 6, such as noise of sensor, precision of sensor, and deformation. This problem will be solved in Section 5.5.

5.2. Geometric Constraint. Force act on the surface of manipulator, so mathematical direction of whole outline is necessary to constraint solution, that is,

$$S(\mathbf{c}) = 0. \tag{27}$$

$S(\cdot)$ means mathematical direction of manipulator surface.

5.3. Normal Vector Constraint. Because that force can only apply to manipulator from outside, the angle of force direction and normal vector is less than $\pi/2$. Based on this constraint, equation could be shown as

$$\mathbf{p}^{T}\mathbf{n} < 0. \tag{28}$$

5.4. Current Mutation Constraint. Strange geometries of manipulator surface and multiple degrees of freedom of manipulator may cause different force action with the same data of force/torque sensor. In this condition, uniqueness solution could not be calculated, so current mutation constraint is drawn in.

Assuming collision point is on the ith joint, then the current of this joint will change suddenly. In addition, the current of kth ($k - i < 0$) joint also produces mutation, but the current of kth ($k - i > 0$) joint will not change suddenly. In this law, collision point will be judged on the ith joint.

On the one hand, this constraint avoids multiple solutions, and on the other hand, it could ensure the range of collision point and accelerate the speed of calculation.

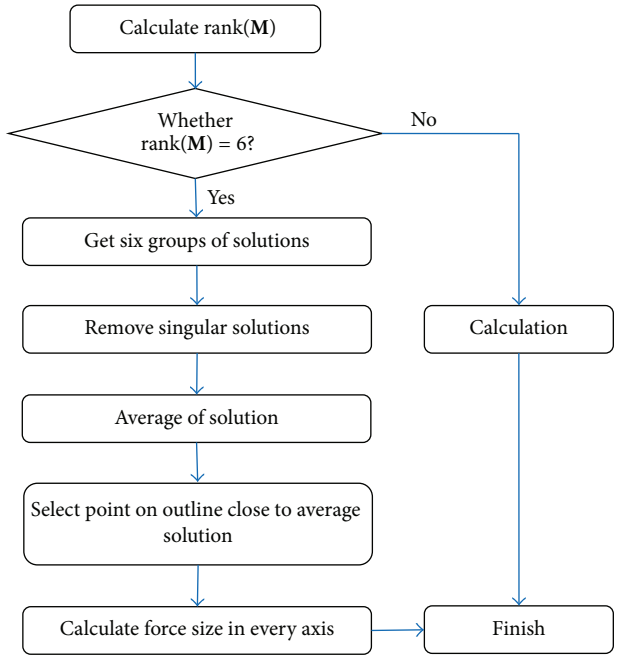

Figure 5: Process of compatibility.

5.5. Compatibility Solution Analysis. In Section 5.1, if rank($\mathbf{M}$) = 5, then uniqueness solution will be achieved combining with (9) which means compatibility is the best. But many elements cause rank($\mathbf{M}$) = 6, such as noise of sensor, precision of sensor, and deformation. There is no solution through combining (8) and (9), so compatibility solution analysis is proposed to ensure an approximate solution. In Figure 5, process of method is shown.

From Figure 5, when rank($\mathbf{M}$) = 6, five equations will be chosen from matrix equation (25) and combining with (9); then one group of solution is obtained. Other five groups of solutions will be also achieved by the same way. Every solution includes the information about position and force size in three coordinate axes. Six normal vectors about solution position are achieved through (25). Then singular solutions should be removed by deviation of positions and normal vectors. At this moment, average values of the rest of solutions are calculated, and choose the closest point in outline of manipulator as approximate solution. At last, force size in three coordinate axes will be achieved by (25). This method avoids no solution condition and achieves an approximate solution.

6. Simulation Experiment

One manipulator with three degrees of freedom is established, as shown in Figure 6. In order to simplify analysis,

Table 1: Parameters of manipulator.

Name	Quality (Kg)	Position of gravity center in local coordinate (mm)
Link 0	1.629	(0, 0, 60)
Link 1	1.786	(0, 0, 69.995)
Link 2	2.565	(86.256, 0, 0)
Link 3	3.180	(106.906, 0, 0)

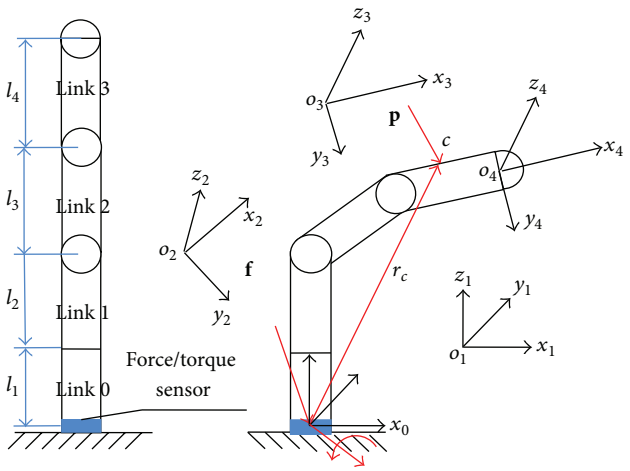

Figure 6: Manipulator structure.

the outline of manipulator is composed of cylindrical surface and semisphere, and the size is set to r_R. In addition, the material of every joint is uniform and set as 1060 alloys (ρ = 2700 kg/m^3) and geometry of every joint is central symmetry; then gravity center of joint lies on central axis.

When collision occurs, data of force/torque sensor change with time. In engineering application, some signal processing methods will be adopted to achieve effective data. In this paper, our attention is focused on the method of collision sensing, so in order to simplify analysis, assume that manipulator is static. Parameters of links are listed in Table 1.

In Figure 6, l_1 = 120 mm, l_2 = 150 mm, l_3 = 200 mm, l_4 = 200 mm, and r_R = 40 mm. Due to the fact that joint connected surface is complex, assume collision point is only on link rod. Surface of each joint is described in coordinate of itself as follows:

Link 1:

$$x_1^2 + y_1^2 = r_R^2, \quad 0 < z_1 \le l_2 - r_R. \tag{29}$$

Link 2:

$$y_2^2 + z_2^2 = r_R^2, \quad r_R \le x_2 \le l_3 - r_R. \tag{30}$$

Link 3:

$$y_3^2 + z_3^2 = r_R^2, \quad r_R \le x_3 \le l_4 - r_R. \tag{31}$$

Top of Link 3:

$$x_4^2 + y_4^2 + z_4^2 = r_R^2, \quad x_4 > 0. \tag{32}$$

According to coordinate transformation matrix as shown in

$$
{}^1_0T = \begin{bmatrix} \cos\theta_1 & -\sin\theta_1 & 0 & 0 \\ \sin\theta_1 & \cos\theta_1 & 0 & 0 \\ 0 & 0 & 1 & l_1 \\ 0 & 0 & 0 & 1 \end{bmatrix},
$$

$$
{}^2_1T = \begin{bmatrix} \cos\theta_2 & 0 & -\sin\theta_2 & 0 \\ \sin\theta_2 & 0 & \cos\theta_2 & 0 \\ 0 & -1 & 0 & l_2 \\ 0 & 0 & 0 & 1 \end{bmatrix},
$$

$$
{}^3_2T = \begin{bmatrix} \cos\theta_3 & -\sin\theta_3 & 0 & l_3\cos\theta_3 \\ \sin\theta_3 & \cos\theta_3 & 0 & l_3\sin\theta_3 \\ 0 & 0 & 1 & 0 \\ 0 & 0 & 0 & 1 \end{bmatrix},
\tag{33}
$$

$$
{}^4_3T = \begin{bmatrix} 1 & 0 & 0 & l_4 \\ 0 & 1 & 0 & 0 \\ 0 & 0 & 1 & 0 \\ 0 & 0 & 0 & 1 \end{bmatrix},
$$

equations of links' outline in basic coordinate will be obtained as shown in the following:

Link 1:

$$(x_1\cos\theta_1 - y_1\sin\theta_1)^2 + (x_1\sin\theta_1 - y_1\cos\theta_1)^2 = r_R^2, \quad l_1 < z_1 \le l_1 + l_2 - r_R. \tag{34}$$

Link 2:

$$(x_2A + y_2B)^2 + (l_1 + l_2)^2 = r_R^2, \quad (l_1)C < x_2C - y_2B \le (l_1 + l_2 - r_R)C. \tag{35}$$

Link 3:

$$\begin{aligned} &(x_3(c\theta_3A + s\theta_3C) - y_3(c\theta_3C - s\theta_3A) + l_3s\theta_3C \\ &\quad + l_3c\theta_3A)^2 + (l_1 + l_2 + z_3)^2 = r_R^2, \\ &r_R(c\theta_3C - s\theta_3A) - l_3s\theta_3A + l_3c\theta_3C \le x_3(c\theta_3C \\ &\quad - s\theta_3A) - y_3(c\theta_3A + s\theta_3C) - l_3s\theta_3A + l_3c\theta_3C \\ &\quad \le (l_4 - r_R)(c\theta_3C - s\theta_3A) - l_3s\theta_3A + l_3c\theta_3C. \end{aligned} \tag{36}$$

Table 2: Different point experiment.

Number	Force size (N)	Force direction (N)	Force position (mm)	Detected force (N)	Detected torque (N·m)	Calculated position (mm)	Calculated force (mm)	Force size error (%)	Force direction error (°)	Position error (%)
1	100	93.8152 9.9627 33.158	40 0 150	−93.8152 79.8145 −33.158	−25.4134 −12.746 6.654	40.34 0.05 152.38	93.1473 10.2345 32.153	0.930	2.087	1.78
2	100	60.9138 74.9999 25.7783	0 40 175	−60.9183 14.7773 −25.7783	−14.8139 −10.6599 9.4891	2.12 39.83 176.33	59.2332 74.5389 25.2234	1.507	2.657	2.017
3	100	−90.4417 42.0904 −6.9776	40 0 200	90.4417 47.6868 6.9776	−18.4897 17.8092 5.3689	42.98 1.46 197.94	−89.1347 40.6234 −7.7463	1.739	3.069	3.187
4	100	73.5958 10.5043 −66.8828	65.02 37.54 267.16	−73.5958 79.2729 66.8828	−21.5907 −24.0106 9.1323	68.58 40.24 263.34	71.3748 9.0657 −66.1635	2.255	4.019	3.632
5	100	−4.7869 94.594 −32.0789	83.75 2.17 312.5	4.7869 4.8169 32.0789	2.7225 −1.1907 −0.8801	85.63 2.37 324.49	−5.0375 96.4736 −34.785	2.677	4.867	4.349
6	100	−36.4847 −68.9913 62.5226	118.66 68.51 302.92	36.4847 158.7685 −62.5226	−52.09 18.4709 12.7395	124.94 63.89 306.35	−35.8134 −70.7645 65.386	2.789	5.032	4.310
7	100	−81.5353 44.681 36.8185	186.93 61.74 442.98	81.5353 45.0962 −36.8185	−9.3882 43.001 −6.3337	174.65 68.49 452.76	−83.4756 44.9652 39.8583	2.853	5.582	5.943
8	100	79.8215 38.4423 −46.3758	210.36 121.45 475.56	−79.8215 51.3349 46.3758	−2.9938 −47.7155 8.6602	222.08 131.75 487.74	82.9467 40.8643 −45.7643	3.171	6.111	6.404
9	100	−80.1006 58.8915 10.7551	206.08 72.79 525.46	80.1006 30.8856 −10.7551	3.2545 44.3061 −10.9144	219.79 84.86 539.75	−84.4754 58.4393 10.4637	3.251	7.457	7.041
10	100	−74.0921 −18.1331 −64.665	222.17 128.27 587.74	74.0921 107.9102 64.665	−29.2707 29.1803 1.5773	238.57 113.45 572.84	−76.4836 −21.9574 −68.4833	4.985	7.886	7.192

Top of Link 3:

$$\begin{aligned}&\left(l_4C - s\theta_3D + x_4\left(c\theta_3C - s\theta_3A\right) - y_4\left(c\theta_3A + s\theta_3C\right)\right.\\&\quad - l_3s\theta_3A + l_3c\theta_3C\Big)^2 + \left(l_4\left(c\theta_3A\right) + s\theta_3C\right.\\&\quad + x_3\left(c\theta_3A + s\theta_3C\right) - y_3\left(c\theta_3C - s\theta_3D\right) + l_3s\theta_3C\\&\quad \left. + l_3c\theta_3D\right)^2 + \left(l_1 + l_2 + z_4\right)^2 = r_R^2,\\&x_4\left(c\theta_3C - s\theta_3D\right) > 0,\end{aligned} \tag{37}$$

where

$$\begin{aligned}A &= c\theta_1s\theta_2 + s\theta_1c\theta_2,\\B &= c\theta_1c\theta_2 + s\theta_2s\theta_1,\\C &= c\theta_1c\theta_2 - s\theta_2s\theta_1,\\D &= c\theta_1s\theta_2 - s\theta_1c\theta_2.\end{aligned} \tag{38}$$

Considering gravity compensation, the manipulator is analyzed as shown in Figure 7, where $a_1 = 86.256$ mm and $a_2 = 106.906$ mm,

$$\begin{aligned}r_1 &= \left[a_1\cos\theta_1\cos\theta_2, a_1\sin\theta_1\cos\theta_2, l_1 + l_2\right.\\&\quad \left. + a_1\sin\theta_2\right]^T,\\r_2 &= \left[a_1\cos\theta_1\cos\theta_2\right.\\&\quad + a_2\cos\theta_1\cos\theta_3, a_1\sin\theta_1\cos\theta_2\\&\quad \left. + a_2\sin\theta_1\cos\theta_3, l_1 + l_2 + a_1\sin\theta_2 + a_2\sin\theta_3\right]^T.\end{aligned} \tag{39}$$

Mode of manipulator is built in ADAMS, and two groups of data are tested to verify our algorithm.

Assume $\theta_1 = \pi/6$, $\theta_2 = -\pi/6$, and $\theta_3 = -\pi/4$, and 100 N force applies on the surface. Ten points are tested, throughout the entire surface.

In another experiment, assume $\theta_1 = \pi/6$, $\theta_2 = -\pi/6$, and $\theta_3 = -\pi/4$, but force size is changed at the same position $\mathbf{C} =$ (206.08 72.79525.46).

In Tables 2 and 3, force size, force direction, and force position are known and set as input conditions; detected

Table 3: Different force experiment.

Number	Force size (N)	Force direction (N)	Force position (mm)	Detected force (N)	Detected torque (N·m)	Calculated position (mm)	Calculated force (mm)	Force size error (%)	Force direction error (°)	Position error (%)
1	60	−48.0604 35.3349 6.4531	206.08 72.79 525.46	48.0604 54.4423 −6.4531	−8.8104 26.5837 −3.7276	223.53 85.34 542.45	−46.4684 32.2344 7.1736	2.993	8.384	8.257
2	80	−64.0805 47.1132 8.6041	206.08 72.79 525.46	64.0805 42.664 −8.0641	−2.7779 3504449 −7.321	223.44 80.32 543.24	−60.3674 46.6237 9.7344	3.106	7.721	7.498
3	100	−80.1006 58.8915 10.7551	206.08 72.79 525.46	80.1006 30.8856 −10.7551	3.2545 44.3061 −10.9144	219.79 84.86 539.75	−84.4754 58.4393 10.4637	3.251	7.457	7.041
4	120	−96.1208 70.6698 12.9062	206.08 72.79 525.46	96.1028 19.1073 −12.9062	9.287 53.1673 −14.5078	216.45 87.87 535.64	−99.8348 70.7982 10.5374	2.843	7.060	6.261
5	140	−112.1409 82.4482 15.0572	206.08 72.79 525.46	112.1409 7.329 −15.0572	15.3194 62.0285 −18.1011	213.23 85.56 538.97	−113.4532 87.1726 13.2736	3.690	6.620	5.874
6	160	−128.161 94.2265 17.2082	206.08 72.79 525.46	128.161 −4.4493 −17.2082	21.3519 70.8898 −21.6945	213.74 81.46 539.53	−123.7562 95.6352 17.3845	2.634	6.104	5.342
7	180	−144.1812 106.0048 19.3593	206.08 72.79 525.46	144.1812 −16.2276 −19.3593	27.3843 79.751 −25.2879	217.36 76.87 540.37	−149.2352 104.8453 18.4632	3.315	5.726	5.319
8	200	−160.2013 117.7831 21.5103	206.08 72.79 525.46	160.2013 −28.0059 −21.5103	33.4168 88.6122 −28.8813	223.42 78.36 530.75	−155.7297 119.4328 20.5643	2.671	5.201	4.955
9	220	−176.2214 129.5614 23.6613	206.08 72.79 525.46	176.2214 −39.7842 −23.6613	39.4493 97.4734 −32.4747	197.45 65.32 535.75	−171.2194 131.3342 22.9472	2.995	5.172	4.637
10	240	−192.2415 141.3397 25.8123	206.08 72.79 525.46	192.2415 −51.5625 −25.8123	45.4817 106.3346 −36.068	199.63 65.37 533.74	−196.24387 140.3484 29.6547	3.082	4.973	3.892

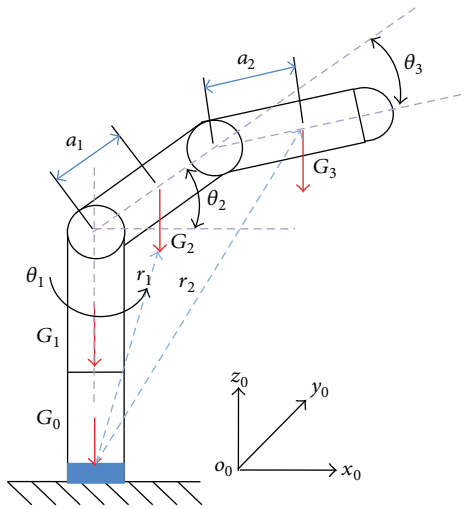

Figure 7: Gravity compensation analysis.

force and detected torque express the data of force/torque sensor, which could be achieved by measurement; calculated position and calculated force could be obtained by (8) and coordinate transformation with a series of calculations; force size error, force direction error, and position error are put forward to judge accuracy and validity of the calculation. Equation of each error is shown as follows:

Force size error:

$$\Delta S = \frac{\left|\sqrt{f_{sx}^2 + f_{sy}^2 + f_{sz}^2} - \sqrt{f_{cBx}^2 + f_{cBy}^2 + f_{cBz}^2}\right|}{\sqrt{f_{cBx}^2 + f_{cBy}^2 + f_{cBz}^2}}. \quad (40)$$

Force direction error:

$$\Delta\theta = \arccos\left(\left|\frac{f_{sx}f_{cBx} + f_{sy}f_{cBy} + f_{sz}f_{cBz}}{\sqrt{f_{sx}^2 + f_{sy}^2 + f_{sz}^2}\sqrt{f_{cBx}^2 + f_{cBy}^2 + f_{cBz}^2}}\right|\right). \quad (41)$$

Position error:

$$\Delta P = \frac{|x_{cB} - x_{sB}| + |y_{cB} - y_{sB}| + |z_{cB} - z_{sB}|}{\sqrt{x_{cB}^2 + y_{cB}^2 + z_{cB}^2}}. \quad (42)$$

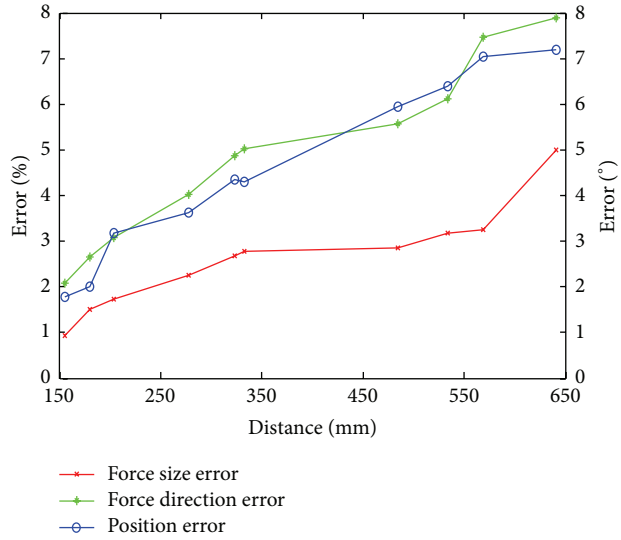

Figure 8: Relation between collision positions and errors.

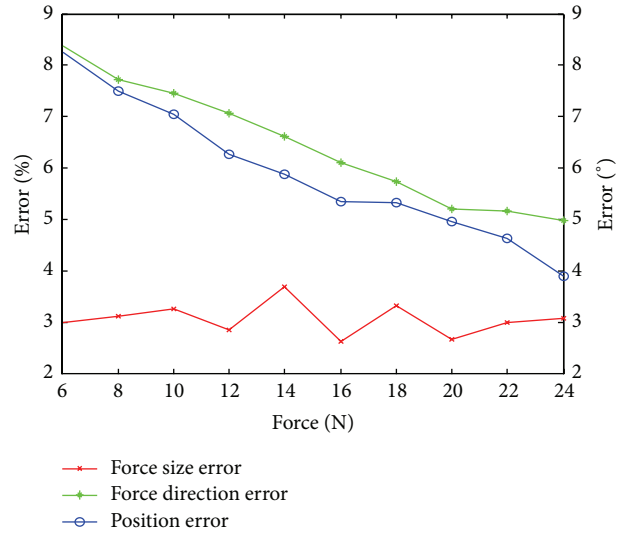

Figure 9: Relation between force and errors.

In these three equations, f_{sx}, f_{sy}, and f_{sz} mean force size of calculated force and x_{sB}, y_{sB}, and z_{sB} mean calculated position mapping to three axes in basic coordination; f_{cBx}, f_{cBy}, and f_{cBz} mean force size of force and x_{cB}, y_{cB}, and z_{cB} mean calculated position mapping to three axes in basic coordination.

From Tables 2 and 3, collision detection is effective and the relative error is extremely small in simulation environment. In order to intuitively express data relation, Figures 8 and 9 are drawn to show them. In Figure 8, relation between different collision positions and each error is established. In Figure 9, relation between different force sizes and each error is established.

In Figure 8, force size error, force direction error, and position error all become larger with farther distance. Different collision point produces different error and each error will be larger with farther distance. If we use this method to test collision information, it must ensure whether the biggest errors meet accuracy requirements at the farthest point of manipulator.

In Figure 9, force direction error and position error become smaller with bigger force, and force size error is fluctuating. Sensitivity of this method is almost certain at the same point, so force direction error and position error become smaller with bigger force. About fluctuating of force size error, (40) has given our explanation that numerator and denominator influence force size error at the same time and have the same trend.

7. Summary

Both animal's arm and person's arm are wrapped by skins, which help them protect their biological organization and apperceive environmental information, such as temperature change and object collision. Researchers except manipulators also have the same function with biological arm, but the method is expensive and easily damaged by distributing sensors on the whole manipulator's outline, so one indirect method to detect collision point and direction by using force/torque sensor is put forward. Compared to skin force sensor, the force/torque sensor is easy to be installed and maintained. In our method, constraint equations and compatibility solution analysis is used to ensure existence of solution. Moreover, gravity compensation and dynamic compensation are also described, which indicate this theory could be effective in gravity environment and when manipulators are exercising. At last, the simulation experiment is executed to verify our algorithm and the result is perfect.

But there exist a lot of engineering problems, if this method is used in real system, which could be as follows: (1) how to extract more accurate force and torque information, based on the fact that signal of sensor is fluctuant; (2) how to describe manipulator's outline accurately, because it has complex shape; (3) how to measure force and torque in an instant when manipulator collides; (4) how to realize real-time perception, on the condition that this theory contents a lot of calculations. In order to promote the theory in engineering application some experiments will be done on a real system, especially putting focus on the above problems.

Conflict of Interests

The authors declare that there is no conflict of interests regarding the publication of this paper.

Acknowledgment

This work is supported by National Postdoctoral Foundation of China under Grant 2013M541258, State Key Laboratory of Robotics (2015-Z08).

References

[1] J. Shi, H. Wu, and Z. Ma, "Design of a new robot skin," *Robot*, vol. 35, no. 1, pp. 32–38, 2013.

[2] M. I. Tiwana, A. Shashank, S. J. Redmond, and N. H. Lovell, "Characterization of a capacitive tactile shear sensor for application in robotic and upper limb prostheses," *Sensors and Actuators A: Physical*, vol. 165, no. 2, pp. 164–172, 2011.

[3] R. Hong, "Compliant control on six axis manipulator," *Robot*, vol. 22, no. 3, pp. 143–147, 2000.

[4] Y. Huang, W. Lu, X. Zhao, C. Lian, and Y. Ge, "Design and experiment of flexible multi-functional tactile sensors for robot skin," *Robot*, vol. 33, no. 3, pp. 347–359, 2011.

[5] T. Someya, Y. Kato, T. Sekitani et al., "Conformable, flexible, large-area networks of pressure and thermal sensors with organic transistor active matrixes," *Proceedings of the National Academy of Sciences of the United States of America*, vol. 102, no. 35, pp. 12321–12325, 2005.

[6] L. Wang, T. Ding, and P. Wang, "Research on stress and electrical resistance of skin-sensing silicone rubber/carbon black nanocomposite during decompressive stress relaxation," *Smart Materials and Structures*, vol. 18, no. 6, Article ID 065002, 2009.

[7] L. Zhang, W. He, and Y. Jian, "Research of bionic skin sensor for robot," *Robot*, vol. 21, no. 4, pp. 309–311, 1999.

[8] Y. Huang, X. Ming, and B. Xiang, "Two types of flexible tactile sensor arrays of robot for three-dimension force based on piezoresistive effects," in *Proceedings of the IEEE International Conference on Robotics and Biomimetics*, pp. 2775–2779, February 2009.

[9] T. Tsujimura and T. Yabuta, "Object detection by tactile sensing method employing F/T information," in *Proceedings of the International Conference on Robotics and Automation*, pp. 444–450, Scottsdale, Ariz, USA, April 1989.

[10] M. Mason and J. Salisbury, *Robot Hands and the Mechanical of Manipulation*, MIT Press, 1985.

[11] A. Bicchi, J. Salisbury, and D. Brock, *Contact Sensing from Force Measurement*, MIT Press, 1990.

[12] X. Zhou, Q. Shi, and Z. Li, "Contact localization using force/torque measurements," in *Proceedings of the 13th IEEE International Conference on Robotics and Automation*, vol. 2, pp. 1339–1344, IEEE, Minneapolis, Minn, USA, April 1996.

[13] X. Zhou, Z. Li, and Q. Zhang, "Tactile sensation based on wrist force sensor," *Robot*, vol. 19, no. 4, pp. 265–270, 1997.

[14] Z. Han, T. Wang, Y. Zhang, and J. Liu, "Selection of calculation model for contact sensing of robot hand using force/torque measurement," *Journal of Beijing University of Aeronautics and Astronautics*, vol. 30, no. 5, pp. 400–404, 2004.